Magnetic properties and electronic origin of the interface between dilute magnetic semiconductors with orthogonal magnetic anisotropy

Ryan F. Need [1,2] Seul-Ki Bac,[3,4] Xinyu Liu [3] Sanghoon Lee,[4] Brian J. Kirby [2] Margaret Dobrowolska,[3] Jacek Kossut [5] and Jacek K. Furdyna[3]

[1]*Department of Materials Science and Engineering, University of Florida, Gainesville, Florida 32611, USA*
[2]*NIST Center for Neutron Research, National Institute of Standards and Technology, Gaithersburg, Maryland 20899, USA*
[3]*Department of Physics, University of Notre Dame, Notre Dame, Indiana 46556, USA*
[4]*Department of Physics, Korea University, Seoul, 136-701, Korea*
[5]*Institute of Physics, Polish Academy of Sciences, 02-668 Warsaw, Poland*

Controlling changes in magnetic anisotropy across epitaxial film interfaces is an important prerequisite for many spintronic devices. For the canonical dilute magnetic semiconductor GaMnAs, magnetic anisotropy is highly tunable through strain and doping, making it a fascinating model system for exploration of anisotropy control in a carrier-mediated ferromagnet. Here, we have used transmission electron microscopy and polarized neutron reflectometry to characterize the interface between GaMnAs-based layers designed to have anisotropy vectors oriented at right angles from one another. For a bilayer of $Ga_{1-x}Mn_xAs_{1-y}P_y$ and $Ga_{1-x}Mn_xAs$, we find that the entirety of the $Ga_{1-x}Mn_xAs$ layer exhibits in-plane magnetic anisotropy and that the *majority* of the $Ga_{1-x}Mn_xAs_{1-y}P_y$ exhibits perpendicular anisotropy. However, near the $Ga_{1-x}Mn_xAs$ interface, we observe a thin Mn-rich region of the nominally perpendicular $Ga_{1-x}Mn_xAs_{1-y}P_y$ that instead exhibits *in-plane* anisotropy. Using first-principles energy considerations, we explain this sublayer as a natural consequence of interfacial carrier migration.

I. INTRODUCTION

Dilute magnetic semiconductors based on Mn-doped III-V compounds and exemplified by GaMnAs have tunable magnetic anisotropy, making them a model system to study exchange coupling in structures where the magnetic anisotropy changes abruptly across an interface [1,2]. The Mn doping levels in these materials are low (typically $\leqslant 10\%$ [3]), which results in Mn-Mn dipole interactions and shape anisotropy 1 to 2 orders of magnitude weaker than conventional metallic ferromagnets [4]. As a consequence of its weak shape anisotropy, GaMnAs is highly susceptible to changes in magnetocrystalline and magnetoelastic anisotropy. In particular, considerable research has been done to establish a quantitative relationship between epitaxial strain and magnetic anisotropy in these systems [3,5]. When locked to GaAs (001) substrates, GaMnAs exists in a compressive biaxial strain state (0.3%) that results in an in-plane (IP) easy axis [6,7]. In contrast, when GaMnAs is tensile strained—for example, when grown on a relaxed InGaAs or ZnCdSe buffer—the easy axis rotates to orient out-of-plane (OP) [2,8–10]. It has also been shown that tensile strain and OP magnetic anisotropy can also be achieved through phosphorous substitution on the V site and the formation of quaternary $Ga_{1-x}Mn_xAs_{1-y}P_y$ alloys [11–14].

More recently, the strain-tunable magnetic anisotropy in $Ga_{1-x}Mn_xAs_{1-y}P_y$ was used to create epitaxial bilayers with orthogonal magnetic anisotropy combinations (i.e., a layer with IP anisotropy adjacent to a layer with OP anisotropy). Specifically, $Ga_{1-x}Mn_xAs_{1-y}P_y/Ga_{1-x}Mn_xAs$ bilayers were grown on GaAs using low-temperature molecular beam epitaxy. Magnetic characterization of these bilayers using SQUID magnetometry and ferromagnetic resonance (FMR) confirmed that such bilayer structures retain components with both IP and OP MA [15]. Additionally, these studies showed that strong interlayer coupling between the epilayers results in an exchange biaslike shift of the hysteresis loop [15,16], similar to that previously observed in IP/OP transition metal multilayers [17–19]. The combination of highly tunable magnetic anistropy and unusual exchange bias make $Ga_{1-x}Mn_xAs_{1-y}P_y/Ga_{1-x}Mn_xAs$ bilayers an ideal system to study the interplay of these effects, and uncover design criteria to generate the interfacial magnetic anistropy needed for specific spintronic applications [20,21].

In the present study, we use transmission electron microscopy (TEM) and polarized neutron reflectometry (PNR) to examine the depth-dependent magnetic order, and specifically the magnetic anisotropy, in a $Ga_{1-x}Mn_xAs_{1-y}P_y/Ga_{1-x}Mn_xAs$ bilayer that exhibits orthogonal magnetic anisotropy. Interestingly, while TEM reveals a sharp bilayer interface and magnetometry identifies two distinct magnetic phases (one with IP anisotropy and one with OP anisotropy), our PNR results reveal a distinct interfacial layer that forms between the nominal $Ga_{1-x}Mn_xAs$ and $Ga_{1-x}Mn_xAs_{1-y}P_y$ layers. To explain the existence and size of this layer, we propose a model of self-limiting hole

redistribution during growth, similar to the formation of a *pn* junction, that changes Mn site occupancy in the interfacial layer. From our PNR results, we estimate the composition and strain of this interfacial layer to be Mn-rich (relative to the adjacent layers), but tensile strained, due to the overwhelming presence of P dopants. Despite this tensile strain, for which we expect OP anisotropy, we observe clear IP anisotropy in PNR, suggesting interlayer exchange coupling and/or magnetic domain structures play a critical role in determining the magnetic behavior of the interfacial layer.

II. EXPERIMENTAL

A. Sample preparation and structural characterization

The $Ga_{1-x}Mn_xAs_{1-y}P_y/Ga_{1-x}Mn_xAs$ bilayer used in this study was grown on GaAs (001) using low-temperature molecular beam epitaxy [22]. Mn concentration of $x = 0.06$ and P concentration of $y = 0.20$ were chosen to achieve compressive strain in the $Ga_{1-x}Mn_xAs$ and tensile strain in the $GaMn_xAs_{1-y}P_y$. For simplicity, these $Ga_{1-x}Mn_xAs$ and $Ga_{1-x}Mn_xAs_{1-y}P_y$ layers are hereafter abbreviated GaMnAs and GaMnAsP, respectively. Following deposition, the film was annealed in vacuum at $270\,^\circ$C for 1 hr to maximize the Curie temperature. Figure 1(a) shows a high-angle annular dark-field (HAADF) TEM image of the sample along the GaAs [110] zone axis. In HAADF imaging, brighter contrast indicates higher atomic Z number [23], and therefore layers with P doping appear darker. Contrast between the epilayers reveals a sharp chemical interface between the GaMnAs and GaMnAsP films, allowing us to unambiguously characterize the layer thicknesses as 12.5 and 21 nm, respectively. Also apparent in Fig. 1(a) are stacking faults along {111} planes that originate at the free GaMnAsP surface and terminate just prior to the GaMnAsP/GaMnAs interface. While it has been shown that these stacking faults break the IP magnetic anisotropy symmetry between the [110] and [1$\bar{1}$0] directions [24], magnetometry and FMR measurements show that the biaxial tensile strain due to the P doping dominates the magnetic anisotropy, resulting in magnetization with an OP easy axis in the P-doped layer [16].

X-ray diffraction (XRD) and reciprocal space mapping (RSM) shown in Fig. 1(b) and 1(c), respectively, confirm the pseudomorphic growth of the two epilayers. In Fig. 1(b), the peak to the left of the GaAs (004) reflection corresponds to compressively strained GaMnAs, while the peak to the right corresponds to the tensile strained GaMnAsP layer. Similarly, the RSM of the asymmetric ($\bar{2}\bar{2}4$) peak in Fig. 1(c) shows a common in-plane lattice constant indicating that both epilayers are coherently strained to the GaAs substrate without relaxation. Quantitative analysis of the XRD reveals that the GaMnAs and GaMnAsP layers are under 0.14% compressive and 0.48% tensile strain, respectively. Experimental Mn and P concentrations ($x = 0.06$; $y = 0.23$) were determined from the lattice constants along the growth direction using Vegard's law. As a final check of the bilayer structure, the specular (00L) XRD pattern was simulated using the chemical concentrations, strain conditions, and thicknesses determined from XRD and TEM as inputs. The result, plotted as the red curve
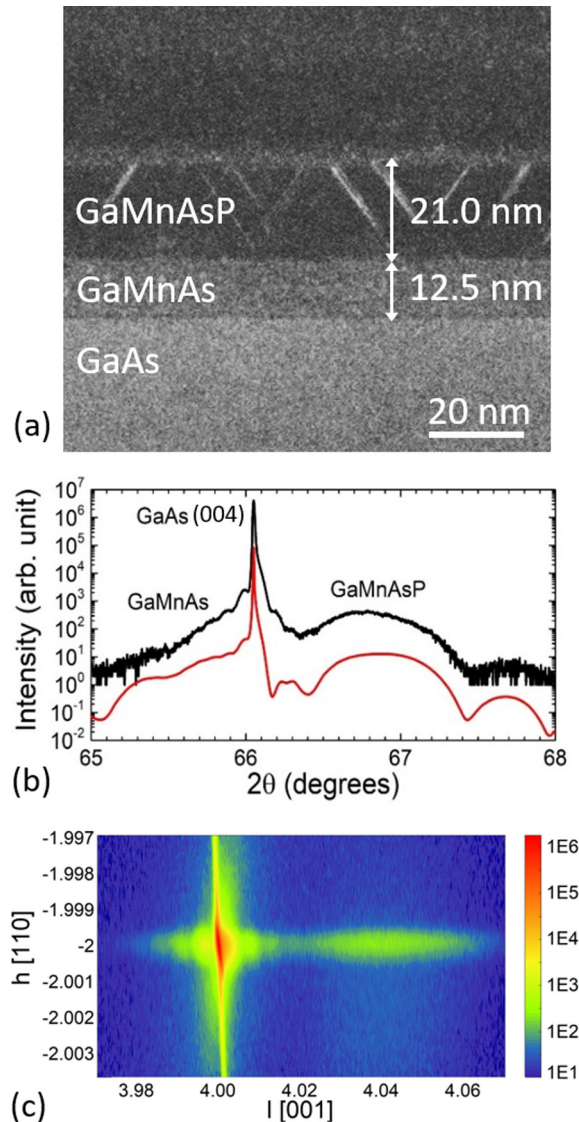

FIG. 1. Structural characterization of the annealed $Ga_{1-x}Mn_xAs_{1-y}P_y/Ga_{1-x}Mn_xAs$ bilayer sample. (a) Cross-sectional high-angle annular dark-field TEM image viewed along the [110] zone-axis projection of the GaAs (001) substrate. (b) XRD spectrum along the (00L) direction. The red curve is a simulated diffraction pattern for the quantitative structure described in the main text and is intentionally offset from the data for clarity. (c) Reciprocal space map taken at the asymmetric ($\bar{2}\bar{2}4$) Bragg peak.

in Fig. 1(b), strongly supports this quantitative description of the bilayer structure.

B. Neutron scattering measurements

SQUID magnetometry measurements of this sample are discussed in detail in Ref. [15]. Those results indicate the presence of two distinct magnetic phases at 5 K, one with IP magnetic anisotropy, and with with OP. However, conventional magnetometry only sees the aggregate contribution (i.e., total magnetization) of a sample, and cannot spatially distinguish distinct magnetic components. In this work, we used PNR measurements to differentiate the IP and OP regions and
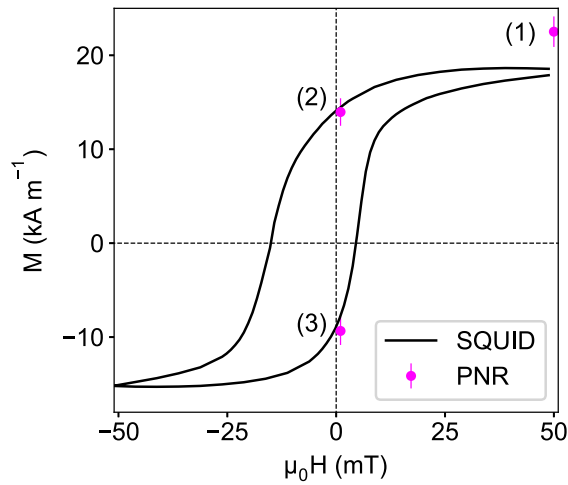
FIG. 2. In-plane magnetization vs in-plane applied magnetic field for the (Ga,Mn)(As,P) bilayer. The sweep starts at the top right-hand quadrant, descending down the top branch, and then ascending up the bottom branch. Numbered points correspond to PNR measurements and the order in which they were collected. The fourth PNR measurement was conducted at $+500$ mT, outside the domain of the figure.

characterize them individually. More specifically, our PNR measurements, collected using the PBR beamline at the NIST Center for Neutron Research, allow us to quantify the depth profiles of the nuclear composition and the in-plane magnetization and thereby define where along the sample's growth axis the chemical and magnetic interfaces occur (note that out-of-plane magnetization is not directly detectable in this geometry). Neutrons are also a particularly sensitive probe to small concentrations of Mn, as Mn characteristic scattering length is negative, while those of Ga, As, and P are all positive [25]. In all of our PNR experiments, a magnetic field H was applied parallel to the sample surface, and the incident beam was polarized with neutron moment aligned either parallel (up, $+$) or antiparallel (down, $-$) to H. The non-spin-flip reflectivities R^{++} and R^{--} were measured as functions of wave-vector transfer along the surface normal Q. The data were reduced using the online REDUCTUS package [26], and the nuclear and magnetic depth profiles were deduced by model fitting of the data using the REFL1D package [27,28]. The data taken at different fields were simultaneously fit to a single consistent model. For this work, all data error bars correspond to one standard deviation while those associated with fitting parameters correspond to two standard deviations.

PNR spectra were measured at 5 K at multiple fields along a minor hysteresis loop associated with exchange bias in this sample [15] and shown in Fig. 2, with integrated magnetizations determined from PNR shown overlaid. First, the sample was field-cooled to 5 K under a $+1$ mT IP field. The field was then ramped to 50 mT, corresponding to (1) in Fig. 2, and PNR was measured. Next, the field was dropped to a near-remanent $+1$ mT, and PNR was remeasured (2). The field was then cycled to -50 mT and back to $+1$ mT, where PNR was remeasured (3). Lastly, PNR was measured in a saturating field of $H = +500$ mT (measurement 4, not shown in Fig. 2). The fitted data are shown in Fig. 3, plotted as spin
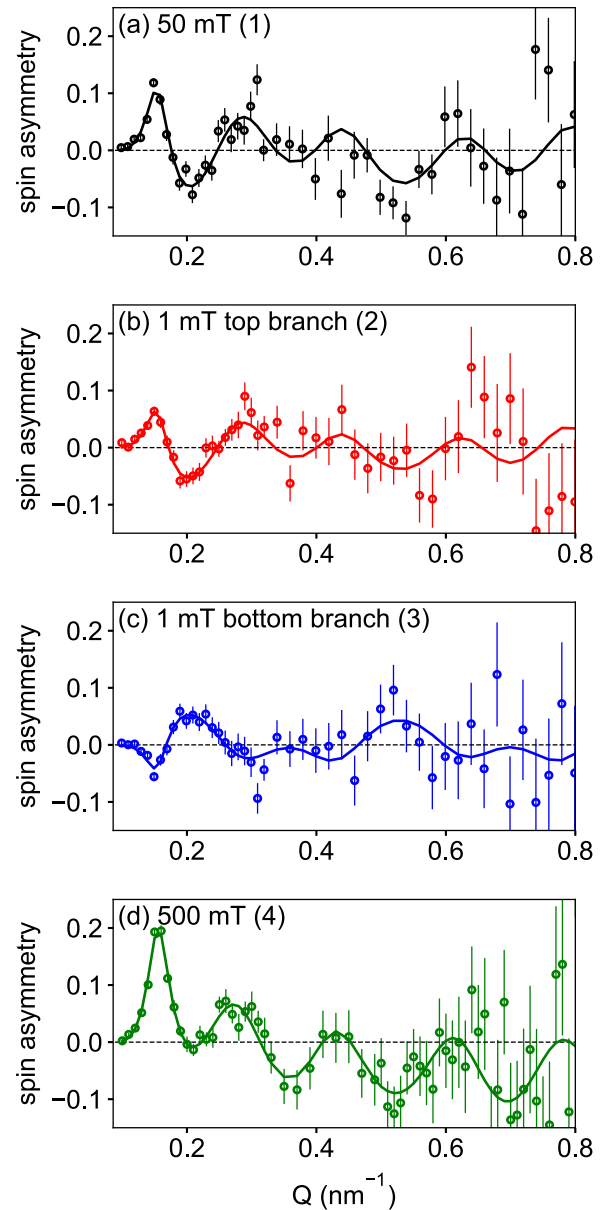

FIG. 3. Fitted PNR data plotted as spin asymmetry, measured at 5 K for the four field conditions described above (a)–(d).

asymmetry (the difference between R^{++} and R^{--} divided by the sum). The same fits plotted on a standard logarithmic scale can be found in Ref. [29].

Since spin asymmetry goes to zero as the magnetization approaches zero, it is a useful quantity for visualizing changes in the magnetic contribution to PNR data, particularly when the magnetization is weak, as is the case here. Moreover, as the nuclear depth profile should not change significantly with field (we do find that it changes slightly, due to slow growth of a contamination layer on the sample surface), changes in the spin asymmetry can be qualitatively associated with changes in sample magnetization, even without quantitative fitting. At 50 mT, Fig. 3(a), we observe a small amplitude oscillation out to $Q = 0.8$ nm^{-1}, demonstrating sensitivity to the magnetic depth profile. As the field is dropped to $+1$ mT, Fig. 3(b), we see a significant reduction in asymmetry

amplitude, associated with a net reduction in magnetization. After cycling to a negative field and coming up the bottom branch to +1 mT 3(c), the signal has largely reversed sign with respect to Fig. 3(b), but is not perfectly antisymmetric to Fig. 3(b). This shows that the magnetization is mostly reversed compared to Fig. 3(b), but that the depth profiles are not precise mirror images of one another. In a quasisaturating 500-mT field, the sign of the low-Q peak switches back to positive, with significantly larger amplitude than seen in Fig. 3(a). This indicates another reversal of magnetization, and that the magnetic profile changes profoundly between 50 and 500 mT.

While we can reach some conclusions based on qualtiative inspection, quantitative information comes from model fitting of the data. From the fits to the data in Fig. 3, we extract the depth profile models shown in Fig. 4. The dashed vertical line through all three panels delineates the nominal GaMnAsP/GaMnAs interface determined from TEM. Critically, we find that the GaMnAsP layer is not uniform. Instead, there is a chemically and magnetically distinct layer at the GaMnAs interface that is approximately 6 nm thick (see Ref. [29] for comparison to a two-slab GaMnAsP/GaMnAs model). In Fig. 4, panels (a) and (b) show the nuclear component of the scattering length density (ρ) and provides a picture of the sample's chemical structure. Moving positively in distance from the GaAs substrate ($z = 0$), we first see a drop in ρ indicative of the GaMnAs layer, followed by a further drop in ρ at the nominal GaMnAsP/GaMnAs interface, followed after 6 nm by an increase in ρ, and finally by an approximately 4-nm-thick surface layer. Note that this surface layer changed slowly over the course of the measurements (which took several days) and is likely attributable to progressive condensation of contaminant gas on the sample surface.

The IP magnetization profiles at 5 K are shown in Fig. 4(c). At 500 mT (4), the magnetization of the entire GaMnAsP layer, including the Mn-rich interfacial layer, is uniform within statistical uncertainty and distinctly larger than that of the underlying GaMnAs. This difference is somewhat counterintuitive, since the amount of Mn supplied during growth was held constant and correspondingly we might expect the amount of Mn incorporated into the GaMnAsP/GaMnAs to be constant. While fully explaining this difference in GaMnAsP and GaMnAs saturated magnetization is beyond the scope of this work, we note that it is consistent with previous magnetometry measurements showing that at moderately strong fields, the magnetization of GaMnAsP specimens is higher than in GaMnAs with the same Mn content [30]. At lower fields (1)–(3), we see that the opposite is true— the majority of the GaMnAsP layer exhibits a smaller IP magnetization than that of the GaMnAs. That the GaMnAsP magnetization decreases faster with reduction of IP field than the GaMnAs magnetization directly demonstrates that the GaMnAs layer indeed exhibits greater IP anisotropy [31,32]. Additionally, at low fields, the interfacial GaMnAsP sublayer magnetization is both larger than that of the rest of the GaMnAsP, and more similar to that of the GaMnAs layer. Since this is not the case at 500 mT, we conclude that the interfacial GaMnAsP sublayer exhibits weaker OP anisotropy than does the rest of the layer. In short, our PNR measurements confirm that the GaMnAs layer and the bulk of the GaMnAsP layer
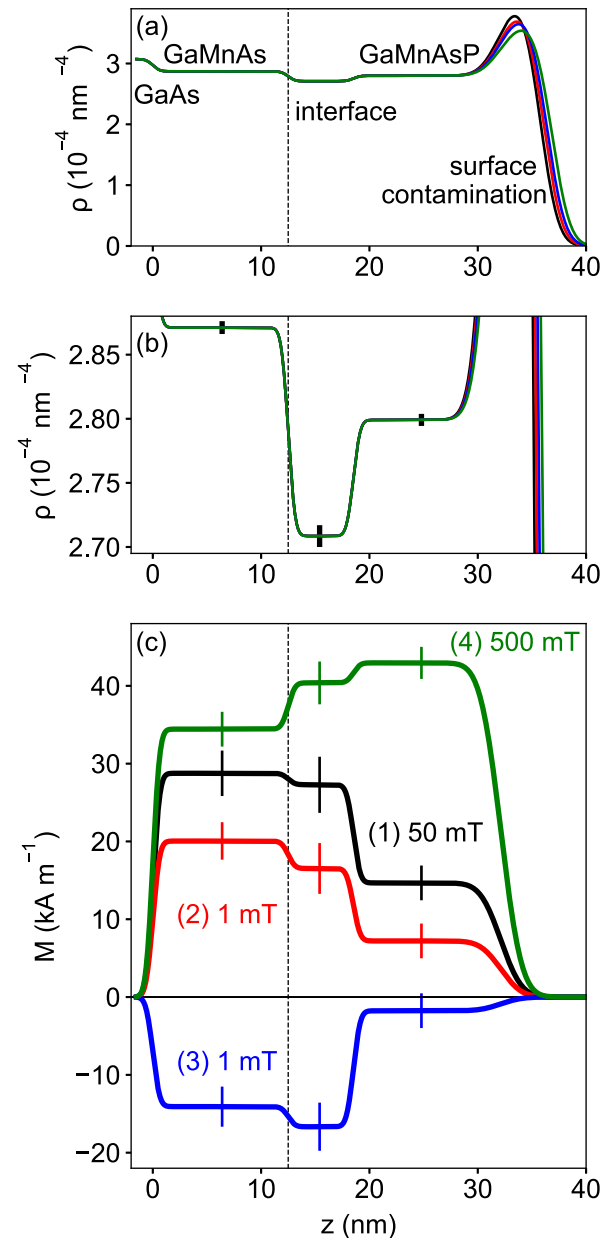

FIG. 4. Scattering length density depth profiles determined from fits to the PNR data. Dashed vertical line delineates the interface between the GaMnAs and GaMnAsP as revealed by TEM. (a) Nuclear profiles indicating chemical interfaces between the layers. (b) Zoom-in of (a), highlighting the chemically distinct interfacial GaMnAsP sublayer. (c) Field-dependent magnetization depth profiles. Error bars on the profiles represent 95% confidence intervals of the fit parameter.

exhibit IP and OP anisotropy, respectively, as expected from prior bulk magnetometry measurements [15]. However, we unexpectedly find a chemically distinct interfacial GaMnAsP sublayer that displays IP anisotropy, despite TEM measurements that show it to be clearly P doped.

The lower nuclear ρ of the GaMnAsP interfacial layer suggests an excess of either Mn, P, or some combination of the two. While we cannot determine the precise chemical composition of the interfacial layer, we can use the refined ρ

value to calculate how much excess Mn or excess P would be needed to achieve that SLD, which serve as boundary conditions for the range of possible interfacial compositions. Full details of the calculations can be found in Ref. [29], here we provide a brief summary of those results. In the case of only excess Mn (P = 22.5%), a Mn concentration of 11.7(6)% is needed to match the measured SLD. This approaches the upper bound of Mn solubility, but is still well within reported values [33]. On the other hand, if only excess P is present (Mn = 8%), a P concentration of 50.9(4.8)% is required. This is more than double the P content in the upper GaMnAsP layer determined by XRD and our calculations, and seems unlikely given that the P flux was held constant during growth. Moreover, such a change in P content would produce a clear contrast in the TEM image in Fig. 1(a), yet we observe no such contrast. Therefore the combination of our TEM results and these SLD calculations suggests that the interfacial layer is predominantly Mn-rich, though we cannot rule out a small component of excess P. Additionally, we can extend these composition estimates, combining them with our XRD data, to estimate the strain in the interfacial layer, which we find to be between 0.41% and 1.24% *tensile* strain corresponding to the Mn and P excess scenarios, respectively. The key point here is that the entire estimated strain range is in the tensile regime, for which we would expect OP magnetic anisotropy rather than the IP anisotropy we observe in PNR. This is a strong indication that interlayer exchange coupling [15] and/or the formation of magnetic domain structures play a critical role in the determination of magnetic anisotropy in this layer.

III. DISCUSSION

While the existence of a unique interfacial layer between GaMnAs and GaMnAsP layers in our sample is an experimental fact, our PNR measurements do not provide a *reason* for the formation of such a well-defined and abrupt interfacial layer. As a starting point to consider possible formation mechanisms, we note that the magnetic behavior of the materials in question are strongly influenced by the ratio of Mn ions substituting for Ga in the crystal lattice (Mn_{Ga}), which act as acceptor centers and produce holes, and Mn atoms in interstitial position (Mn_I), which are compensating donors. Specifically, the presence of Mn_I leads to fewer net magnetic moments, since the positively charged Mn_I are loosely bound and diffuse into the proximity of the negatively charged Mn_{Ga} sites where, by antiferromagnetic exchange interaction, they compensate the Mn_{Ga} magnetic moments. The presence of Mn_I also leads to weaker magnetic interactions between the remaining magnetic moments, since the number of mobile holes is compensated by the electrons coming from Mn_I double donors. For these two reasons, the formation of Mn_I has a strongly detrimental effect on the ferromagnetism of GaMnAs.

The Mn_{Ga}/Mn_I ratio depends on the value of the Fermi energy of holes present in the materials [34]. That is, when the Fermi level of holes produced by Mn_{Ga} reaches a sufficiently high value, it becomes energetically more favorable to form Mn_I than to add additional Mn_{Ga} acceptors that form additional holes. To understand the relevance of this behavior in

our bilayer, we note that the valence band edges in GaAs and GaP are offset by about 0.4 eV, with the latter being situated lower in energy. From this we can estimate that the top of the valence band of GaMnAsP at 23% of P will be about 0.1 eV below that of GaMnAs. Thus, as GaMnAsP is deposited on top of GaMnAs, any holes present in GaMnAsP will drift toward to the GaMnAs region forming an accumulation of positive charge on the GaMnAs side. This spatial transfer of holes will continue until an energy balance is achieved between the valence band offset and the Coulomb attraction exerted by the negatively charged ionized acceptor cores remaining in the layer from which the holes were transferred. In turn, this competition leads naturally to a finite length scale for the depletion region in GaMnAsP, where our interfacial layer resides.

We can attempt to estimate the thickness of an interfacial layer formed in this way by assuming that the hole transfer is stopped when the potential of the charged slab at its surface reaches the value equal to the offset between the hole energy levels in the two adjacent materials. Taking the number of the transferred holes to be on the order of 10^{20} cm^{-3} and the valence band offset amounts to 0.1 eV, one ends up with the value of 15 nm for the thickness of the interfacial layer containing an enhanced concentration of Mn_{Ga}. One should bear in mind that the rate of change of Mn_{Ga}/Mn_I with changing Fermi level is at present impossible to estimate in a quantitative manner. Furthermore, the high Mn concentrations dealt with here mean that the impurity band formed in this material is expected to have an effective mass distinctly different from the valence band in (Ga,As)(Mn,P), again making these arguments primarily qualitative in character. Thus, while it is difficult to quantitatively correlate the changes in the number of transferred holes (i.e., changes of the Fermi energy of the holes) with the number of additional Mn_{Ga}, it is reasonable to assume it to be equal to or less than 10^{20} cm^{-3}, in which case, our rough estimate yields an interfacial layer thickness that is in order-of-magnitude agreement with that observed in our PNR data.

Another ramification of our model is that when holes are transferred out from the interfacial GaMnAsP region during growth, the Fermi level in that region will be reduced and enable the incorporation of a higher fraction of Mn_{Ga}, which will boost magnetization by increasing both the number of magnetic moments and the strength of the interaction between them. This agrees with the lower SLD value of the interfacial layer found in our PNR refinements. However, the hole transfer is not expected to affect the number of Mn_{Ga} in GaMnAs, since the growth of that layer is already complete and the lattice positions of Mn ions are stable. It is worth emphasizing that it is not the subtle spatial transfer of holes toward GaMnAs that is itself responsible for the changes of the magnetic properties of the interfacial layer. Instead, this hole transfer perturbs the ratio of the Mn_{Ga} sites to Mn interstitials, which, in turn, profoundly changes the magnetism of the interfacial layer.

We recognize that our model involves a number of oversimplifications. In particular, one has to remember that the picture of the band structure in GaMnAs and related compounds must include the formation of the Mn-related impurity band. In fact, there is strong evidence that the Fermi level

is located in such a band [35–37]. The question thus arises: what is the impurity band discontinuity when interfacing GaMnAs and GaMnAsP? The roughest estimate is that this level remains fixed in distance from the vacuum level, independent of the host material. However, by comparing various experimental data [36,37] and theoretical results [38–42], one notices that the impurity level varies considerably and qualitatively tracks the top of the valence band. Therefore, while the impurity band offset is somewhat smaller than the corresponding valence band offset (e.g., 0.1 eV vs. 0.4 eV in the case of GaAs and GaP), the impurity band can still nonetheless promote the transfer of holes from the GaMnAsP to the GaMnAs layer during the growth process, validating our qualitative picture.

Thus far, we have not focused on the role of magnetic domain structures in our results, primarily because PNR has a limited ability to resolve domain structure in our sample. In specular PNR measurements, as performed in this study, scattering information is collected purely along the sample normal direction resulting in a one-dimensional depth profile in which in-plane variations (e.g., changes in magnetic SLD arising from magnetic domains) are averaged out. We can however consider domain structures distributed vertically throughout our sample. Of particular interest here is the possible identification of closure domains or pinned spins near the GaMnAsP/GaMnAs interface that have been hypothesized to explain the exchange bias observed in this system [16], as well as other systems with orthogonal magnetic anisotropy [17–19]. Exchange bias is this geometric configuration necessarily requires the formation of closure domains at the interface of the two materials, as shown by Choi *et al.* While such closure domains must reside on the GaMnAsP side of the bilayer, magnetically they should reflect the easy-axis IP anisotropy of the GaMnAs layer, which is precisely the behavior we observe in the interfacial layer revealed by PNR. It is therefore logical to speculate that the interfacial layer observed in PNR and the closure domains observed in magnetotransport are closely related. In Ref. [29], we compare fitting of models based on different possible domain configurations. Unfortunately, due to the limited Q range over which we measured, and the small contrast of the magnetization differences involved, negligible fit improvement was seen in models featuring full closure domains or models with pinned interfacial moments. Further investigation, for example via Lorentz TEM, is needed to more conclusively elucidate the connection between our interfacial layer, the magnetic domain structure, and exchange bias in this system.

IV. CONCLUSIONS

In conclusion, we have combined TEM, XRD, and PNR measurements to characterize the chemical and magnetic depth profiles of a bilayer heterostructure composed of the dilute magnetic semiconductor systems (Ga,Mn)As and (Ga,Mn)(As,P). Our magnetic depth profiles confirm that the GaMnAs layer exhibits IP and while the bulk of the GaMnAsP layer exhibits OP anisotropy, as expected from bulk magnetization measurements and the known effect of P doping on strain-induced magnetic anisotropy. A key finding of our work is the existence of an interfacial layer between the GaMnAsP and GaMnAs layers that—despite P doping—displays IP anisotropy. To explain this interfacial layer, we propose a qualitative model of hole transfer during growth that modifies the Mn dopant site distribution, changing the ratio of substitutional to interstitial dopants, and with it, the expected magnetization behavior. This hole transfer is intrinsically limited by Coulomb attraction across the depletion region leading to a finite size for this interfacial layer, which our simple model predicts to be on the order of our experimental result (15 nm vs. 6 nm, respectively). While PNR cannot resolve the in-plane magnetic domain structure, the IP anisotropy of this interfacial layer matches the behavior of closure domains that have been hypothesized as the origin of exchange bias in multilayers with orthogonally oriented magnetic anisotropy. Future studies to isolate and identify closure domains, in this system and other orthogonally coupled magnetic multilayers, will be important for controlling magnetic anisotropy and exchange bias for spintronic applications.

ACKNOWLEDGMENTS

[1] H. Ohno, Science **281**, 951 (1998).

[2] S. Lee, J.-H. Chung, X. Liu, J. K. Furdyna, and B. J. Kirby, Mater. Today **12**, 14 (2009).

[3] T. Dietl and H. Ohno, Rev. Mod. Phys. **86**, 187 (2014).

[4] J. Zemen, J. Kučera, K. Olejník, and T. Jungwirth, Phys. Rev. B **80**, 155203 (2009).

[5] X. Liu and J. K. Furdyna, J. Phys.: Condens. Matter **18**, R245 (2006).

[6] S. Kim, H. Lee, T. Yoo, S. Lee, S. Lee, X. Liu, and J. K. Furdyna, J. Appl. Phys. **107**, 103911 (2010).

[7] H. Ohno, A. Shen, F. Matsukura, A. Oiwa, A. Endo, S. Katsumoto, and Y. Iye, Appl. Phys. Lett. **69**, 363 (1996).

[8] A. Shen, H. Ohno, F. Matsukura, Y. Sugawara, N. Akiba, T. Kuroiwa, A. Oiwa, A. Endo, S. Katsumoto, and Y. Iye, J. Cryst. Growth **175-176**, 1069 (1997).

[9] S. Chung, D. Shin, H. Kim, S. Lee, X. Liu, and J. Furdyna, J. Electron. Mater. **37**, 912 (2008).

[10] K. Tivakornsasithorn, T. Yoo, H. Lee, S. Choi, S. Lee, X. Liu, M. Dobrowolska, and J. K. Furdyna, Solid State Commun. **253**, 37 (2017).

[11] A. Lemaître, A. Miard, L. Travers, O. Mauguin, L. Largeau, C. Gourdon, V. Jeudy, M. Tran, and J.-M. George, Appl. Phys. Lett. **93**, 021123 (2008).

[12] A. W. Rushforth, M. Wang, N. R. S. Farley, R. P. Campion, K. W. Edmonds, C. R. Staddon, C. T. Foxon, and B. L. Gallagher, J. Appl. Phys. **104**, 073908 (2008).

[13] M. Cubukcu, H. J. von Bardeleben, K. Khazen, J. L. Cantin, O. Mauguin, L. Largeau, and A. Lemaître, Phys. Rev. B **81**, 041202(R) (2010).

[14] H. Lee, J. Chang, P. Chongthanaphisut, S. Lee, S. Choi, S.-K. Bac, A. R. Nasir, S. Lee, A. Pardo, S. Dong, X. Li, X. Liu, J. K. Furdyna, and M. Dobrowolska, AIP Adv. **7**, 055809 (2017).

[15] X. Li, S.-K. Bac, S. Dong, X. Liu, S. Lee, S. Rouvimov, M. Dobrowolska, and J. K. Furdyna, AIP Adv. **8**, 056401 (2018).

[16] S. Choi, S.-K. Bac, X. Liu, S. Lee, S. Dong, M. Dobrowolska, and J. Furdyna, Sci. Rep. **9**, 1 (2019).

[17] J. Sort, A. Popa, B. Rodmacq, and B. Dieny, Phys. Rev. B **70**, 174431 (2004).

[18] A. Bollero, V. Baltz, L. D. Buda-Prejbeanu, B. Rodmacq, and B. Dieny, Phys. Rev. B **84**, 094423 (2011).

[19] D. Navas, J. Torrejon, F. Béron, C. Redondo, F. Batallan, B. P. Toperverg, A. Devishvili, B. Sierra, F. Castaño, K. R. Pirota, and C. A. Ross, New J. Phys. **14**, 113001 (2012).

[20] V. P. Amin, J. Zemen, and M. D. Stiles, Phys. Rev. Lett. **121**, 136805 (2018).

[21] J. Wunderlich, B.-G. Park, A. C. Irvine, L. P. Zârbo, E. Rozkotová, P. Nemec, V. Novák, J. Sinova, and T. Jungwirth, Science **330**, 1801 (2010).

[22] J. Sadowski, R. Mathieu, P. Svedlindh, J. Z. Domagała, J. Bak-Misiuk, K. Światek, M. Karlsteen, J. Kanski, L. Ilver, H. Åsklund, and U. Södervall, Appl. Phys. Lett. **78**, 3271 (2001).

[23] E. Carlino, S. Modesti, D. Furlanetto, M. Piccin, S. Rubini, and A. Franciosi, Appl. Phys. Lett. **83**, 662 (2003).

[24] M. Kopecký, J. Kub, F. Máca, J. Mašek, O. Pacherová, A. W. Rushforth, B. L. Gallagher, R. P. Campion, V. Novák, and T. Jungwirth, Phys. Rev. B **83**, 235324 (2011).

[25] I. S. Anderson, P. J. Brown, J. M. Carpenter, G. Lander, R. Pynn, J. M. Rowe, O. Schärpf, V. F. Sears, and B. T. M. Willis, in *International Tables for Crystallography*, 1st ed., edited by E. Prince (International Union of Crystallography, Chester, England, 2006) Vol. C, pp. 430–487.

[26] B. Maranville, W. Ratcliff II, and P. Kienzle, J. Appl. Cryst. **51**, 1500 (2018).

[27] B. Kirby, P. Kienzle, B. Maranville, N. Berk, J. Krycka, F. Heinrich, and C. Majkrzak, Curr. Opin. Colloid Interface Sci. **17**, 44 (2012).

[28] B. B. Maranville, A. Green, and P. A. Kienzle, arXiv:1801.04975.

[29] See Supplemental Material at http://link.aps.org/supplemental/10.1103/PhysRevMaterials.4.054410 for additional magnetometry data showing the effect of sample annealing, comparison of magnetic domain structure PNR models, and discussion of the composition and strain in the interfacial layer.

[30] X. Li, Investigation and Manipulation of Ferromagnetic Properties of GaMnAs and GaMnAsP Nanostructures, Ph.D. thesis, University of Notre Dame, 2017 .

[31] B. J. Kirby, J. E. Davies, K. Liu, S. M. Watson, G. T. Zimanyi, R. D. Shull, P. A. Kienzle, and J. A. Borchers, Phys. Rev. B **81**, 100405(R) (2010).

[32] B. J. Kirby, P. Greene, B. B. Maranville, J. Davies, and K. Liu, J. Appl. Phys. **117**, 063905 (2015).

[33] S. Mack, R. Myers, J. Heron, A. Gossard, and D. Awschalom, Appl. Phys. Let. **92**, 192502 (2008).

[34] T. Dietl, D. D. Awschalom, M. Kaminska, and H. Ohno, *Spintronics* 1st ed. (Academic Press, 2008), Chap. 3, p. 89.

[35] M. Dobrowolska, K. Tivakornsasithorn, X. Liu, J. Furdyna, M. Berciu, K. Yu, and W. Walukiewicz, Nat. Mater. **11**, 444 (2012).

[36] M. Tanaka, S. Ohya, and P. Nam Hai, Appl. Phys. Rev. **1**, 011102 (2014).

[37] J. Okabayashi, A. Kimura, O. Rader, T. Mizokawa, A. Fujimori, T. Hayashi, and M. Tanaka, Physica E **10**, 192 (2001).

[38] P. Mahadevan and A. Zunger, Appl. Phys. Lett. **85**, 2860 (2004).

[39] K. S. Burch, D. D. Awschalom, and D. N. Basov, J. Magn. Magn. Mater. **320**, 3207 (2008).

[40] R. Bouzerar and G. Bouzerar, Europhys. Lett. **92**, 47006 (2010).

[41] T. Graf, M. Gjukic, M. Brandt, M. Stutzmann, and O. Ambacher, Appl. Phys. Lett. **81**, 5159 (2002).

[42] M. A. Mayer, P. R. Stone, N. Miller, H. M. Smith, III, O. D. Dubon, E. E. Haller, K. M. Yu, W. Walukiewicz, X. Liu, and J. K. Furdyna, Phys. Rev. B **81**, 045205 (2010).